



UNIVERSITAT POLITÈCNICA
DE CATALUNYA
BARCELONATECH

UPCommons

Portal del coneixement obert de la UPC

<http://upcommons.upc.edu/e-prints>

© 2015. Aquesta versió està disponible sota la llicència CC-BY-NC-ND 4.0 <http://creativecommons.org/licenses/by-nc-nd/4.0/>

© 2015. This version is made available under the CC-BY-NC-ND 4.0 license <http://creativecommons.org/licenses/by-nc-nd/4.0/>

Manuscript Number: SOLMAT-D-14-01082R2

Title: Enhanced stability in semi-transparent PTB7/PC71BM photovoltaic cells

Article Type: Regular Manuscript

Keywords: PTB7, OSC, stability, Warburg, inverted, Photonic crystal

Corresponding Author: Dr. PABLO ROMERO-GOMEZ,

Corresponding Author's Institution: ICFO

First Author: PABLO ROMERO-GOMEZ

Order of Authors: PABLO ROMERO-GOMEZ; RAFAEL BETANCUR, DR.; ALBERTO MARTINEZ-OTERO; MARINA MARIANO; XAVIER ELIAS; BEATRIZ ROMERO, DR.; BELÉN Arredondo; RICARDO Vergaz; jordi martorell

Abstract: We studied the performance over time of opaque and semi-transparent PTB7:PC71BM bulk hetero-junction solar cells. For unsealed inverted configuration cells we observe that when the isolation from the environment is improved, the degradation observed is dominated by one single exponential decay. We demonstrate that a dielectric multilayer stack of approximately 550 nm provides an isolation that increases the lifetime of the cell close to ten times. In that event the fill factor appears to be the PV parameter dominating cell degradation resulting from a decrease in the shunt resistance. An Impedance analysis we performed indicates that a Warburg element, attributed to the presence of slowly moving charges such as heavy ions, must be included in the description of the experimental data. The contribution from such element increases as the cell degrades in good agreement with a degradation dominated by the corrosive effects from external agents reaching the active layer of the device.

Frederik Christian Krebs, Ph.D.
Editor
Solar Energy Materials and Solar Cells

Dear Professor F. Krebs,

Please find enclosed the revised version of the manuscript with Ms. Ref. No.: SOLMAT-D-14-01082R1 entitled "Enhanced stability in semi-transparent PTB7/PC71BM photovoltaic cells" which we are submitting for your consideration to be published in Solar Energy Materials and Solar Cells.

We have revised our manuscript according to the comments and suggestions from both reviewers. Enclosed with the manuscript we provide a detailed response to the reviewers points. Essentially, we do not have any strong disagreement with the reviewers remarks and we used their comments and suggestions to improve the manuscript. In response to the request of an ISOS-L-1 test made by reviewer#3, we provide a supplementary data file which is cited in the revised main text. With the submission we provide a detailed response to the reviewers points and an indication of the changes introduced. Additionally, we provide a copy of the text where all changes introduced are in blue.

We would like to use this opportunity to thank you again for all the time and consideration dedicated to our manuscript.

Sincerely yours,

Dr. Pablo Romero-Gomez
ICFO - Institut de Ciències Fotòniques
Parc Mediterrani de la Tecnologia
08860 Castelldefels (Barcelona)
T: 34 93 5534049
e-mail: pablo.romero@icfo.es
web: <http://www.icfo.es>

January 1, 2014

Response to reviewers

Reviewer #1: The manuscript by Romero-Gomez and coworkers describes semitransparent BHJ solar cells made with the PTBT:PC71BM blend. It is shown that (i) inverted structures exhibit an enhanced stability (well-known), (ii) the 500 nm thick MoO₃/MgF₂ multi-layer blocks the absorption of air in semitransparent solar cells (expected with that thickness), (iii) the absorption of air induces a ionic conduction in the considered cells. The most valuable results of the study could be the impedance spectroscopy (IS) characterization. However,

(i) the behaviour of the impedance spectra with the applied voltage is not shown

Response:

Three new figures have been added to the manuscript showing the time evolution of the impedance at 0, 0.4 and 0.8 V respectively.

In the first paragraph in page 6 of the revised manuscript the following sentence is included:

For $V < 0,6$ V the Warburg feature is not observed and therefore R_w is set to 0.

The second paragraph in page 6 has been rewritten as follows:

Nyquist plots at four different voltages are shown in figures 6 as examples of impedance measurements for three different times. We observe a good agreement between the experimental data and the theoretical fit. The main feature in the complex plane is a typical depressed semicircle in the medium-high frequency range, a standard behaviour in organic solar cells associated to carrier recombination. The semicircle diameter increases with time, which implies an increase of the parallel resistance R_p . This leads to a corresponding rise of the recombination time and therefore to an enhancement of the carrier density. Besides, the semicircle depression is more pronounced with time, leading to a decrease of CPE_p parameter, and thus moving away from the ideal capacitor behaviour. At low frequencies, for $V = 0.6$ and 0.8 V, one may observe a tail associated to a Warburg behaviour that is more pronounced as time evolves. This results in an increase of the Warburg resistance, obtaining values of $R_w = 148.3$ (98.6) Ω at $t=0$, $R_w = 447.6$ (237.8) Ω at $t=1176$ h and $R_w = 683$ (311) Ω at $t=2232$ h for $V=0.6$ (0.8) V.

(ii) the choice of the equivalent circuit of Figure 6b is not motivated (at least some Refs)

Response:

The circuit model has been chosen taking into account the shape of the Cole-Cole diagram. R-CPE circuit models the semi-depressed semicircle and Warburg element models the feature found at low frequencies (for 0.6 and 0.8 V). We added references 23, 24 and 25 that use the same equivalent circuit and observe the same behaviour in Cole-Cole diagrams:

(iii) the impedance spectra for all the investigated cell structures are not compared,

Response:

As we demonstrate in our work the stability of non-encapsulated solar cells is affected by the penetration of slow moving charges. In that respect the impedance spectra do not show significant differences when the degree of isolation is changed.

(iv) the representation of the impedance spectra is not correct (IS spectra must be plotted in a square plot with the same range, in order to evaluate the circle depression, as well as the slope of the low-frequency features, attributed to a Warburg impedance),

Response:

As correctly pointed by the reviewer it is customary to represent the impedance spectra using the same range in both axes. However, in our study, especially for measurements taken at 0.6 V and 0.8 V, the CPE_p can become less than 0.9. For this reason, we decided to use different ranges.

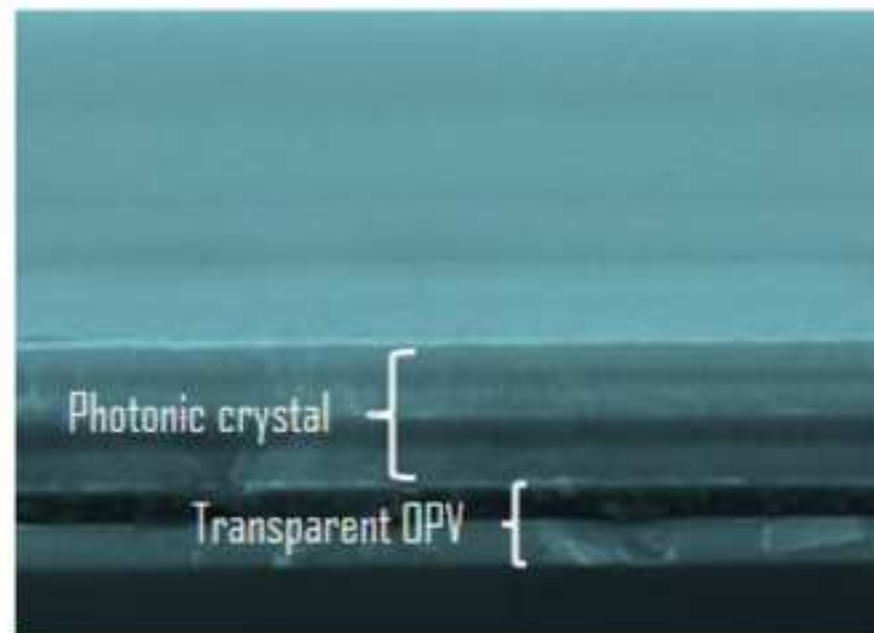
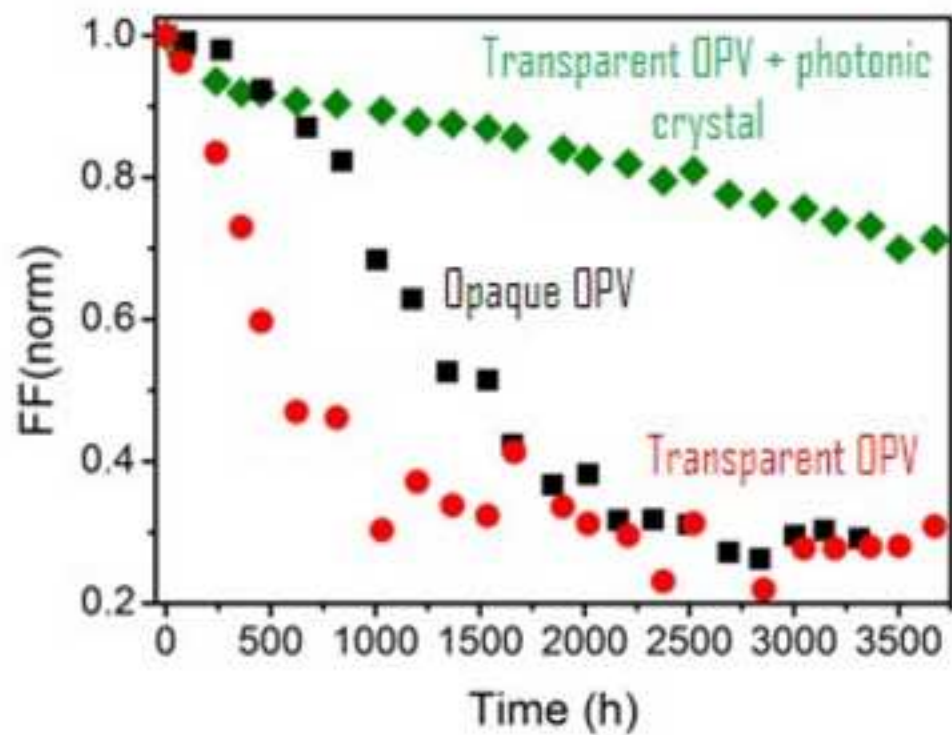
(v) the slope of the Warburg component is not given.

Response:

We agree with the reviewer that the Warburg coefficient can be derived from the slope of the plot Z vs $t^{-1/2}$, in the event that we had obtained a semi-infinite Warburg impedance. In our case the impedance plot shows a tail towards the x axis, indicating a finite diffusion. Thus, it is more appropriate fitting such behaviour to a short-circuit Warburg impedance. Indeed, the Warburg resistance is a more convenient parameter to show the trend of the diffusion process with time.

Reviewer #3: I quite like this manuscript that is well illustrated and described. The written english could be improved in places but from the technical point of view it is OK. The long terms stability that the authors describe under ISOS-D-1 is acceptable but they should mandatorily show ISOS-L-1 or similar. PTB-7 is known to be unstable but maybe their multilayer structure improves it slightly. I am convinced the authors did the experiment, but did not like the result. It is important that the PTB-7 story is told correctly.

We appreciate the comments and suggestions from the reviewer. In accordance, we performed ISOS-L-1 tests which are commented in lines 9-15 form page 8 of the revised manuscript. The data corresponding to such tests is provided in the supplementary data file.



- Influence of the OPV stability on the penetration of degradation agents as, for instance, moisture.
- Performance over time of opaque and semi-transparent PTB7:PC71BM bulk hetero-junction solar cells.
- Incorporation of a 1-D multilayer structure to enhance the lifetime of organic cells.

Enhanced stability in semi-transparent PTB7/PC71BM photovoltaic cells

Pablo Romero-Gomez,^{a*} Rafael Betancur,^a Alberto Martinez-Otero,^a Xavier Elias,^a Marina Mariano,^a Beatriz Romero^b, Belén Arredondo^b, Ricardo Vergaz^c, and Jordi Martorell^{a,d}

a- ICFO-Institut de Ciències Fòtiques, Mediterranean Technology Park, 08860 Castelldefels (Barcelona), Spain.

b- Escuela de Ciencias Experimentales y Tecnología, Universidad Rey Juan Carlos, 28933 Móstoles (Madrid), Spain.

c- Escuela Politécnica Superior, Universidad Carlos III de Madrid, 28911 Leganés (Madrid), Spain.

d- Departament de Física i Enginyeria Nuclear, Universitat Politècnica de Catalunya, Terrassa, Spain.

*corresponding author: pablo.romero@icfo.es

Keywords: PTB7, OSC, stability, Warburg, inverted, Photonic crystal

We studied the performance over time of opaque and semi-transparent PTB7:PC71BM bulk hetero-junction solar cells. For unsealed inverted configuration cells we observe that when the isolation from the environment is improved, the degradation observed is dominated by one single exponential decay. We demonstrate that a dielectric multilayer stack of approximately 550 nm provides an isolation that increases the lifetime of the cell close to ten times. In that event the fill factor appears to be the PV parameter dominating cell degradation resulting from a decrease in the shunt resistance. An Impedance analysis we performed indicates that a Warburg element, attributed to the presence of slowly moving charges such as heavy ions, must be included in the description of the experimental data. The contribution from such element increases as the cell degrades in good agreement with a degradation dominated by the corrosive effects from external agents reaching the active layer of the device.

1. Introduction

Since the early works on organic solar cells (OSC), many different polymers have been synthesized towards the goal of obtaining an active material with an optimal photon to charge conversion that would make such type of cells a commercially viable technology. In recent years, cells made with bulk hetero-junctions (BHJ) of PTB7/PC₇₁BM have emerged as one of the most promising polymer based devices combining the unique features of an organic based technology with a relatively high power conversion efficiency (PCE) [1],[2]. Interestingly, it has been shown that such polymer blend can be used to obtain high performance homogeneously semi-transparent solar cells [3]. Unlike semi-transparent cells fabricated using other types of polymers or PV technologies, with PTB7 one may fabricate devices which do not alter the colour of the objects seen through them. However, despite the high PCEs obtained and the potential for the PTB7/PC₇₁BM blend to be used in building integrated PV, any

practical application for such cells would be pending on the final stability of the devices fabricated using such blend.

For many different kinds of organic based PV cells it has been reported that the penetration of oxygen and moisture into the active layer of the cell results in severe loss of performance [4],[5],[6],[7],[8]. In the standard OPV configuration, the acidic nature of the poly(3,4-ethylenedioxythiophene):poly(styrenesulphonic acid) (PEDOT:PSS) used as electron blocking layer (EBL) [9],[10] leads the etching of the indium tin oxide (ITO) electrode [11]. For instance, in P3HT oxygen has been demonstrated to react with the side chain by insertion in the alpha position relative to the thiophene ring [12]. In polyfluorenes oxygen insertion next to the quaternary carbon leads to fluorenone units and results in severe damage of the polymer properties [13]. Blocking of similar carbon positions with bulky side chains that prevent oxygen insertion has resulted in important increases in device stability [14], especially when aryl groups are used instead of alkyl chains. Large improvements in the stability of organic devices can be obtained in inverted configurations that bypass the need to use PEDOT:PSS. In such architecture, n-type metal oxides such as ZnO or TiO₂ are deposited on the ITO layer to lower the work function of the electrode [15],[16], while NiO, WO₃ or MoO₃ may be used as EBL [11]. Further improvements in stability may be reached by an adequate isolation from the most aggressive external agents [4].

In the current work we study the stability of cells which use PTB7:PC71BM as the active blend. In particular we show that the incorporation of a 1-D multilayer structure combining three layers of high refractive index (HRI) and two layers of low refractive index (LRI) dielectric materials to enhance the efficiency of semi-transparent cells[3] acts also as an efficient barrier to protect the cell from a rapid degradation. In the first part of the work, a comparison between the stability of opaque and semi-transparent cells is provided. In the second, the performance of opaque and semi-transparent inverted devices is compared, and the impact of the multi-layer structure (ML) over the long term stability is analysed.

2. Experimental

2.1-Device Fabrication

To fabricate the photovoltaic devices we used 120 nm thick ITO-patterned substrates. For the standard configuration, PEDOT:PSS was used as EBL while thermally evaporated BCP as HBL. Details of the preparation of such cells can be found elsewhere [17]. For the inverted solar cells, a thermally evaporated MoO₃ layer was used as EBL while ZnO was used as HBL. The ZnO layer was grown by sol-gel where the precursor solution was prepared according to Ref [18]. Spin coating was performed at 6000 rpm during 60 seconds followed by a thermal annealing at 200°C during 20 min in air. In the semi-transparent devices, a 10 nm thick silver back electrode was thermally evaporated at 5.5 Å s⁻¹ onto a substrate cooled down to -5°C [19]. The thicknesses for all the layers are reported in Table 1 (note that all devices have the same active layer thickness). We fabricated five different types of non-encapsulated PTB7:PC₇₁BM BHJ cell architectures (see figure 1): Standard opaque (Std-Opaque), Standard semi-transparent (Std-ST), inverted opaque (Inv-Opaque), inverted semi-transparent (Inv-ST), and inverted semi-transparent with a multilayer trapping structure (Inv-ML-ST). Thicknesses of the photovoltaic cell layers were determined numerically to optimize light harvesting in the opaque configuration [3],[17],[20] with the only constraints imposed by the fabrication procedures or the charge collection limitations of the materials used. The photovoltaic part and the photonic structure deposited on top of the transparent Ag electrode may be clearly distinguished in the field-emission scanning electron microscopy (FESEM) cross-section view of the Inv-ML-ST device shown in Figure 2.

Table 1 Thicknesses (in nm) for all layers in the five different configurations considered

In order to make Std-ST, Inv-ST, and Inv-ML-ST devices semi-transparent, the back silver contact was made 10 times thinner than for the opaque cells (i.e. 10 nm instead of 100 nm thickness). Std-ST and Inv-ST devices were capped with a 10 nm protective MoO₃ layer deposited on top of the back Ag contact. For the Inv-ML-ST device, such protective layer was replaced by the photonic crystal, a five-layer structure based on MoO₃ (HRI) and MgF₂ (LRI). The structure was designed numerically to provide the adequate light management to

optimize the performance of the cell, i.e. to increase light trapping in the near IR and near UV region. Details on such numerically based optical optimization for semi-transparent cells can be found in Ref. [3], where a similar analysis was applied to optimize the PCE of semi-transparent standard cells.

Fig. 1 Architecture for the OPV devices reported in this work. In all cases illumination was from the substrate side. The opaque samples differ from the transparent ones in the thickness of the Ag back-contact electrode. The blocking layers corresponding to standard and inverted solar cells architectures are indicated on the left and right of the drawings, respectively. Layer thicknesses are not drawn at scale.

2.2 Device characterization.

The PCE of the fabricated devices was determined from current density-voltage curve measurements obtained under 1 sun, AM 1.5G spectrum illumination from a solar simulator (Abet Technologies, model Sun 3000). The solar simulator illumination intensity was monitored using a monocrystal silicon reference cell (Rera Systems) calibrated against a National Renewable Energy Laboratory calibrated reference cell. In the characterization of all semi-transparent cells, illumination was from the ITO side. Impedance Spectroscopy (IS) measurements were performed under illumination conditions using a standard red LED. A Solartron 1260 impedance analyzer was used (Solartron Analytical, Farnborough, UK). The cell was connected to the analyzer that fed the input signal, biasing the device at different dc levels and superimposing an alternating signal with amplitude 100 mV and sweeping frequency from 1 Hz to 1 MHz.

Fig. 2 Schematic and FESEM image of ML-ST. A) Photovoltaic cells were fabricated on top of fused silica glass substrate. The cell area, i.e. the area over which the Ag and ITO electrodes overlap was 0.09 cm^2 . The multilayer photonic structure was deposited on top of the electrical structure saving the silver contacts. B) SEM cross-sectional micrograph of the ML-ST. The photovoltaic structure consists of two parts. On the one hand the electrical part based on PTB7:PCBM-based cell. On the other hand, the multilayered $\text{MoO}_3/\text{MgF}_2$ PC. In this particular case instead of on a glass substrate, the structure was grown on a doped-silicon substrate to avoid charging effects during the SEM scanning.

3. Results and discussion

3.1. Time Evolution of the PV parameters

The study the aging process of the fabricated devices was performed according to the ISOS-standards defined in Ref. [21]. We performed two sets of experiments. In one set we compared the performance of the Std-Opaque and Std-ST configurations relative to the Inv-Opaque one, while in a second set we compared the three different inverted

configurations. The PV parameters for each cell were measured at the start of the aging process (cf. Table 2). All PV parameters measured subsequently were normalized to the corresponding initial values. In between measurements the cells were stored at ambient conditions in the dark, which corresponds to ISOS-D-1 shelf test at level 2 according to consensus stability testing protocols for OPVs[21]. With such level 2 test we aimed at determining the role played by the ML on the lifetime of the cells and determine the origin of cell degradation under such conditions. In our study, the cell lifetime is taken as the time the cell efficiency drops to 80% of its initial value [21].

The time evolution of the main PV parameters (V_{oc} , J_{sc} , FF and PCE) for the first set of time evolution experiments is shown in Figure 3. As it has been reported with other polymer blends, the acidic nature of the PEDOT:PSS in contact with the ITO causes a rapid degradation of the FF and V_{oc} [22]. Such source of rapid degradation may mask any other source of degradation possibly related to the thickness of the capping metal electrodes and consequently we observe that Std-Opaque and Std-ST degrade at a very similar speed. On the contrary, the Inv-ST cells exhibit a lifetime of approximately 250 hours, corresponding to at least 50 times the lifetime of the other two cells.

Fig. 3 Evolution of the PV parameters for Std-Opaque (Wine squares), Std-ST (Blue triangles), and Inv-ST (red circles) solar cells. All parameters are normalized to their respective value at $t=0$ h. The lines are guides for the eye.

In the second set of experiments we considered only the inverse configurations. The evolution of all PV parameters for the three cells under study is shown in Figure 4. As in the previous set of time evolution experiments the cells were stored in air and under darkness in between measurements. For all three inverted cells, the FF exhibits a faster degradation than V_{oc} and J_{sc} . Consequently the efficiency followed, to a large extent, the evolution of the FF. Note that the lifetime for the Inv-Opaque with a capping electrode of 100 nm is 800 hours, close to three times the lifetime of the Inv-ST which is only capped with 10 nm of Ag and 10 nm of MoO_3 . This suggests that external agents are a dominant source of degradation for the inverted cells and that thicker capping layer provide a better isolation from such agents. Note that for the Inv-ST and the Inv-Opaque a sudden drop in FF begins after 50 hours and after 500 hours, respectively. In the 3500 hours of the study, this drop was not observed for the ML-ST cell.

Table 2 PV parameters for five different configurations

To gain further insight in the degradation mechanisms of the latter device, the natural logarithm of the normalized FFs are shown in Figure 5a for the three inverted devices. We observe that for the Inv-ML-ST cell, after an initial transient of approximately 1000 hours, the FF experiences a slow exponential decay with a decay time of 10,500 hours. The degradation in performance for the Inv-ST cell exhibits, first, a fast exponential decay up to approximately 1000 hours, and secondly, a very slow decay time once the cell is already practically dead. The Inv-Opaque exhibits a similar behavior but delayed 500 hours. In such first 500 hours the evolution of such opaque cell is similar to the long exponential decay of the Inv-ML-ST cell. As can be seen in Figure 5a, such long decay observed for the Inv-ML-ST cell can be adjusted to one single exponential, indicating one dominant mechanism of degradation for such devices. By comparing the decay rates for the three different type of devices, shown in Figure 5a, we observe that a larger cell isolation can be associated to a larger cell lifetime indicating that degradation may be linked to the external agents such as oxygen and moisture.

Fig. 4 Evolution of the normalized PV parameters for Inv-Opaque (black squares), Inv-ST (red circles) and ML-ST (blue diamonds) cells: Jsc (a), Voc (b), FF (c), and Eff (d) All parameters are normalized to the respective value at $t = 0$ h. The dotted lines in (d) indicate the time at which the efficiency is 80% of the initial value. The life-times of the Inv-ST/Inv-Opaque/MS-ST cells were approximately 250/750/1900 h.

We monitored the evolution the R_s and R_{sh} for the three devices under study shown in Figures 5b and 5c, respectively. For the Inv-ML-ST device the R_s exhibits a slow increase over time while the R_{sh} degrades faster except for an initial period where that resistance increased slightly. A degradation of the device dominated by the R_{sh} over the R_s is an indication that such degradation is primarily located in the active material. For the Inv-Opaque the thick Ag metal electrode also serves as a barrier to protect the active part, but in this case the barrier is thinner and, once the corrosive agents reach effectively the active layer, the degradation becomes very rapid. For the Inv-ST, the lack of any protection barrier leads to an almost immediate degradation of both, the R_s and R_{sh} .

Fig. 5 Evolution of the (a) natural logarithm of the cell FF, (b) the series resistance and, (c) the shunt resistance for Inv-Opaque (black squares), Inv-ML-ST (green diamond), and Inv-ST (red circles) solar cells.

Additional information from the degradation mechanism can be obtained by measuring the time evolution of impedance on an Inv-Opaque cell at different voltages. Impedance experimental data have been fitted with the

equivalent circuit shown in the inset of Figure 6 in accordance with the model described in ref [23],[24],[25]. It consists of a series resistance, R_s , modelling metallic contacts, wires, etc., and a parallel resistance, R_p , that accounts for the cell dynamical resistance. The circuit also includes a constant phase element (CPE) that is a non-ideal capacitance taking into account non-homogeneities such as porosities, roughness and surface states and it presents an impedance given by $Z_{CPE} = \frac{1}{(CPE_T)(j\omega)^{CPE_P}}$ with CPE_P ranging from 0 to 1 and CPE_T being

approximately the capacitance value (when $CPE_P = 1$). Finally, the circuit includes a Warburg element that models the existence of slowly diffusion charges, typically ions with an associated impedance given by

$$W = \frac{R_W \tanh(j\omega C_T)^{C_P}}{(j\omega C_T)^{C_P}}$$

where R_W is the Warburg resistance associated to the size of the low frequency tail in the

Nyquist plot, C_T is a coefficient related to diffusion effects and C_P is related to roughness of the diffusion media [26]. For $V < 0.6$ V the Warburg feature is not observed and therefore R_W is set to 0.

Fig. 6 Impedance spectra of the Inv-Opaque cell measured at a) 0 V b) 0.4 V c) 0.6 V and d) 0.8 V, and at three different times (solid squares). Solid lines correspond to the theoretical fit. Inset in a) corresponds to the equivalent circuit scheme used to fit the experimental data.

Nyquist plots at four different voltages are shown in figures 6 as examples of impedance measurements for three different times. We observe a good agreement between the experimental data and the theoretical fit. The main feature in the complex plane is a typical depressed semicircle in the medium-high frequency range, a standard behaviour in organic solar cells associated to carrier recombination. The semicircle diameter increases with time, which implies an increase of the parallel resistance R_p . This leads to a corresponding rise of the recombination time and therefore to an enhancement of the carrier density. Besides, the semicircle depression is more pronounced with time, leading to a decrease of CPE_P parameter, and thus moving away from the ideal capacitor behaviour. At low frequencies, for $V = 0.6$ and 0.8 V, one may observe a tail associated to a Warburg behaviour that is more pronounced as time evolves. This results in an increase of the Warburg resistance, obtaining values of $R_W = 148.3$ (98.6) Ω at $t=0$, $R_W = 447.6$ (237.8) Ω at $t=1176$ h and $R_W = 683$ (311) Ω at $t=2232$ h for $V=0.6$ (0.8) V. The increase in R_W suggests an increment in the number of slowly moving charges as the cell degrades attributed to the heavy ions that are being dragged into the active blend by the water that penetrates in the cell as times evolves. This

would be in agreement with a cell degradation dominated by a rapid decrease in the shunt resistance for the opaque cell as we observed in Figure 5c. It is observed that R_w is higher for 0.6 V than for 0.8 V. This could appear bizarre at first glance. However, this should be analysed in comparison with the recombination resistance R_p . The ion diffusion process modelled by R_w cannot be analysed by itself, but always related to the recombination mechanism. In fact, it is the ratio R_w/R_p that gives an idea of the ion diffusion influence on the overall dynamical process. This ratio increases with voltage, being for the last day of measurement 0.18 and 0.24 for 0.6 V and 0.8 V, respectively.

1 This suggests that ion diffusion is linked to carrier recombination, as R_p increases, carrier recombination decreases
2 enhancing carrier density and hindering ion diffusion.
3
4

5 When inverted configuration devices are sealed, penetration of moisture is prevented and the cells exhibit a
6 decay time constant close to 2000 hours. We performed ISOS-L-3 tests and observed, as shown in Figure 1S a of
7 the supplementary data file, that the FF of inverted devices exhibits a two exponential type degradation being the
8 time constant of the rapid one 14 hours and 1960 hours for the slow one. When the UV light from the solar
9 simulator is filtered using a GG400 filter, the rapid degradation disappears and, as shown in Figure 1S b of the
10 supplementary data file, the FF of the cell degrades following an almost single exponential decay with a time
11 constant above 2000 hours.
12
13
14
15
16
17
18
19
20
21
22
23

24 **4. Conclusions**

25
26
27 We have considered the over time performance of five different PTB7:PC₇₁BM cell configurations and concluded
28 that for unsealed devices when isolation from external corrosive elements increases, the degradation becomes
29 clearly dominated by the sole action of such external agents. In such conditions degradation can be directly linked
30 to a decrease in the shunt resistance. Additionally, we performed an impedance study that suggested an increase in
31 the presence of slowly moving charges as the degradation of the cell developed. The partial but rather effective cell
32 isolation we implemented was achieved by the deposition of five layers of dielectrics with a total thickness of 554
33 nm. Lifetimes for inverted semi-transparent cells including such layer stack were close to 8 times the lifetime for
34 equivalent cells without the stack and 400 times larger when compared to standard configuration semi-transparent
35 cells. When comparing semi-transparent devices to opaque ones, the reduced thickness of the metal electrode did
36
37
38
39
40
41
42
43
44
45
46
47
48
49

not seem to have a direct effect on the cell lifetime other than being a less effective barrier to external corrosive agents. For sealed devices where further penetration of such corrosive elements is prevented, degradation appears to be dominated by a photo-degradation that can be slowed down when UV light is filtered out. The time evolution results we reported for cells fabricated with the PTB7:PC71BM blend, clearly indicate that such cells have the potential to become stable in the event that the fabricated devices are properly isolated from the surrounding environment.

1
2
3
4
5
6
7
8
9
10
11
12
13
14
15
16
17
18
19
20
21
22
23
24
25
26
27
28
29
30
31
32
33
34
35
36
37
38
39
40
41
42
43
44
45
46
47
48
49

Acknowledgements

This work was supported by the Ministerio de Economía y Competitividad with the grants MAT2011-28665, IPT-120000-2010-29 and IPT-2012-0986-120000, and we acknowledge support from the EC under the project Solprocel with grant number No. 604506.

References

- [1] L. Lu and L. Yu, Understanding Low Bandgap Polymer PTB7 and Optimizing Polymer Solar Cells Based on It, *Adv. Mater.* 26 (26) (2014) 4413
- [2] Y. Liang, Z. Xu, J. Xia, S.T. Tsai, Y. Wu, G. Li, C. Ray, L. Yu, For the Bright Future—Bulk Heterojunction Polymer Solar Cells with Power Conversion Efficiency of 7.4%, *Adv. Mater.* 22 (20) (2010) 135.
- [3] R. Betancur, P. Romero-Gomez, A. Martinez-Otero, X. Elias, M. Maymo, J. Martorel *Nat. Photonics.* 7 (12) (2013) 995.
- [4] M. Jørgensen, K. Norrman, S. A. Gevorgyan, T. Tromholt, B. Andreasen, F. C. Krebs, Stability of Polymer Solar Cells, *Adv. Mater.* 24 (5) (2012) 580.
- [5] C. H. Peters, I. T. Sachs-Quintana, J. P. Kastrop, S. Beaupre, M. Leclerc, M. D. McGehee, High Efficiency Polymer Solar Cells with Long Operating Lifetimes, *Adv. Energy Mater.* 1 (2011) 491.
- [6] D. Angmo, S. A. Gevorgyan, T. T. Larsen-Olsen, R. R. Søndergaard, M. Hösel, M. Jørgensen, R. Gupta, G. U. Kulkarni, F. C. Krebs, Scalability and stability of very thin, roll-to-roll processed, large area, indium-tin-oxide free polymer solar cell modules, *Org. Electron.* 14 (3) (2013) 984.
- [7] T.Y. Chu, S. W. Tsang, J. Zhou, P. G. Verly, J. Lu, S. Beaupre, M. Leclerc, Y. Tao, High-efficiency inverted solar cells based on a low bandgap polymer with excellent air stability, *Sol. Energy Mater. sol. cells* 96 (1) (2012) 155.
- [8] N. Espinosa, R. Garcia-Valverde, A. Urbina, F. C. Krebs, A life cycle analysis of polymer solar cell modules prepared using roll-to-roll methods under ambient conditions, *Sol. Energy Mater. sol. Cells*, 95 (2011) 1293.
- [9] S. Gunes, H. Neugebauer, N. S. Sariciftci, Conjugated polymer-based organic solar cells, *Chem. Rev.* 107 (4) (2007) 1324.
- [10] S. Woo, W.H. Kim, H. Kim, Y. Yi, H. K. Lyu, Y. Kim, 8.9% Single-Stack Inverted Polymer Solar Cells with Electron-Rich Polymer Nanolayer-Modified Inorganic Electron-Collecting Buffer Layers, *Adv. Energy Mater.* 4 (7) (2014) 1301692 .
- [11] Y. Sun, Ch. J. Takacs, S. R. Cowan, J. HwaSeo, X. Gong, A. Roy, A. J. Heeger, Efficient, Air-Stable Bulk Heterojunction Polymer Solar Cells Using MoOx as the Anode Interfacial Layer, *Adv. Mater.* 23 (19) (2011) 2226.
- [12] M. Manceau, A. Rivaton, J-L. Gardette, Guillerez S, N. Lemaître, The mechanism of photo- and thermooxidation of poly(3-hexylthiophene) (P3HT) reconsidered, *Polym. Degrad. Stab.* 94 (6) (2009) 898.

- 1 [13] R. Grisorio, G. Allegretta, P. Mastrorilli, G. P. Suranna, On the Degradation Process Involving
2 Polyfluorenes and the Factors Governing Their Spectral Stability, *Macromolecules* 44 (20) (2011)
3 7977.
4
- 5 [14] P. C. Yang, J. Y. Sun, S. Y. Ma, Y. M. Shen, Y. H. Lin, C. P. Chen, C. F. Lin, Interface
6 modification of a highly air-stable polymer solar cell, *Sol. Energy Mater. Sol. Cells* 98 (2012) 351.
7
- 8 [15] Z. He, C. Zhong, S. Su, M. Xu, H. Wu, Y. Cao, Enhanced power-conversion efficiency in
9 polymer solar cells using an inverted device structure, *Nat. Photonics*. 6 (9) 2012 591.
10
- 11 [16] Z. Lin, C. Jiang, C. Zhu, J. Zhang, Development of Inverted Organic Solar Cells with
12 TiO₂ Interface Layer by Using Low-Temperature Atomic Layer Deposition, *Appl. Mater. Interfaces*, 5
13 (3) (2013) 713.
14
- 15 [17] A. Martínez-Otero, X. Elias, R. Betancur, J. Martorell, High-Performance Polymer Solar Cells
16 Using an Optically Enhanced Architecture, *Adv. Optical Mater.* 1 (1) 2013 37.
17
- 18 [18] Y. Sun, J. H. Seo, C. J. Takacs, J. Seifert, A. J. Heeger, Polymer bulk heterojunction solar cells:
19 function and utility of inserting a hole transport and electron blocking layer into the device structure,
20 *Adv. Mater.* 23 (14) (2011) 1679.
21
- 22 [19] N. P. Sergeant, A. Hadipour, B. Niesen, D. Cheyngs, P. Heremans, P. Peumans, B. P. Rand *Adv.*
23 *Mater.* 24 (6) (2012) 728.
24
- 25 [20] R. Betancur, A. Martinez-Otero, X. Elias, P. Romero-Gomez, S. Colodrero, H. Miguez, J.
26 Martorell, Optical interference for the matching of the external and internal quantum efficiencies in
27 organic photovoltaic cells, *Sol. Energy Mater. Sol. Cells*, 104 (2012) 87.
28
- 29 [21] M. O. Reese et. al., Consensus stability testing protocols for organic photovoltaic materials and
30 devices, *Sol. Energy Mater. Sol. Cells*, 95 (2011) 1253-1267.
31
- 32 [22] M.P. de Jong, L. J. van IJzendoorn, M.J.A. de Voigt, Stability of the interface between indium-
33 tin-oxide and poly(3,4-ethylenedioxythiophene)/poly(styrenesulfonate) in polymer light-emitting
34 diodes, *Appl. Phys. Lett.* 77 (2000) 2255.
35
- 36 [23] XinhongPeng, Hongbing Yu, Xin Wang, NingshengjieGao, LijuanGeng and Lina Ai, Enhanced
37 anode performance of microbial fuel cells by adding nanosemiconductor goethite, *Journal of Power*
38 *Sources*, 223 (2013) 94-99.
39
- 40 [24] Youzhong Dong, Yanming Zhao, He Duan, Zhiyong Liang, Enhanced electrochemical
41 performance of LiMnPO₄ by Li⁺ conductive Li₃VO₄ surface coatins, *ElectrochimicaActa*, 123
42 (2014) 244-250.
43
- 44 [25] Ruifeng Li, Zhuguo Li, Yanyan Zhu, Kai Qi, Structure and corrosion resistance properties of Ni-
45 Fe-B-Si-Nb amorphous composite coatings fabricated by laser processing, *Journal of Alloys and*
46 *Compounds*, 580 (2013) 327-331.
47
- 48 [26] C. Lopez-Lopez, S. Colodrero, S. R. Raga, H. Lindstrom, F. Fabregat-Santiago, J. Bisquert, H.
49 Miguez *J. Mater. Chem.* 22 (5) (2012) 1751.
50
- 51
52
53
54
55
56
57
58
59
60
61
62
63
64
65

Table 1 Thicknesses (in nm) for all layers in the five different configurations considered

	ITO	PEDOT:PSS	ZnO	BHJ	BCP	MoO₃	Ag	MoO₃/MgF₂
Std-Opaque	120	40	--	100	3.5	--	100	--
Std-ST	120	40	--	100	3.5	--	10	10/0/0/0/0
Inv-Opaque	120	--	30	100	--	5	100	--
Inv-ST	120	--	30	100	--	5	10	10/0/0/0/0
Inv-ML-ST	120	--	30	100	--	5	10	112/136/102/102/102

Table 2 PV parameters for five different configurations

	Jsc (mA/cm²)	Voc (mV)	FF	Efficienc y (%)	LUMINOSITY (%)
Std-Opaque	13.06	714	69	6.43	0
Std-ST	8.31	722	70	4.19	32
Inv-Opaque	13.26	746	73	7.27	0
Inv-ST	8.09	732	74	4.39	31.6
Inv-ML-ST	10.02	745	72	5.37	30.1

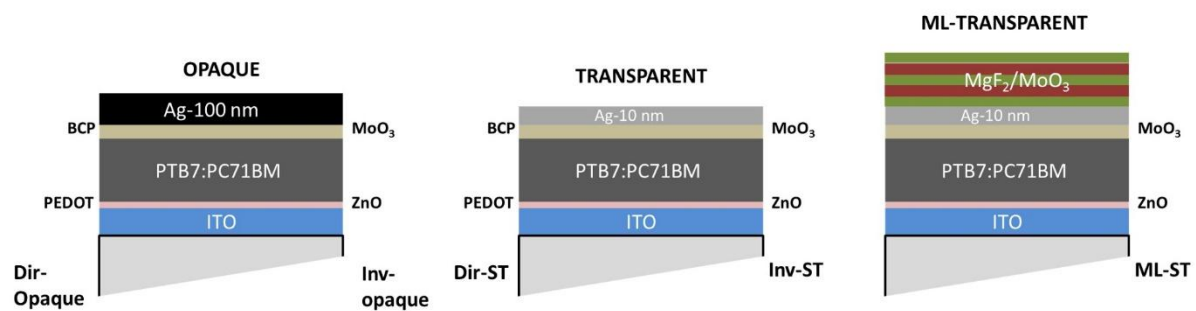


Fig. 1 Architecture for the OPV devices reported in this work. In all cases illumination was from the substrate side. The opaque samples differ from the transparent ones in the thickness of the Ag back-contact electrode. The blocking layers corresponding to standard and inverted solar cells architectures are indicated on the left and right of the drawings, respectively. Layer thicknesses are not drawn at scale.

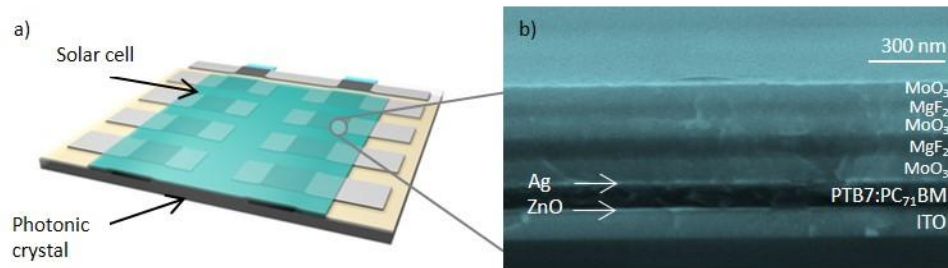


Fig. 2 Schematic and FESEM image of ML-ST. A) Photovoltaic cells were fabricated on top of fused silica glass substrate. The cell area, i.e. the area over which the Ag and ITO electrodes overlap was 0.09 cm^2 . The multilayer photonic structure was deposited on top of the electrical structure saving the silver contacts. B) SEM cross-sectional micrograph of the ML-ST. The photovoltaic structure consists of two parts. On the one hand the electrical part based on PTB7:PCBM-based cell. On the other hand, the multilayered MoO₃/MgF₂ PC. In this particular case instead of on a glass substrate, the structure was grown on a doped-silicon substrate to avoid charging effects during the SEM scanning.

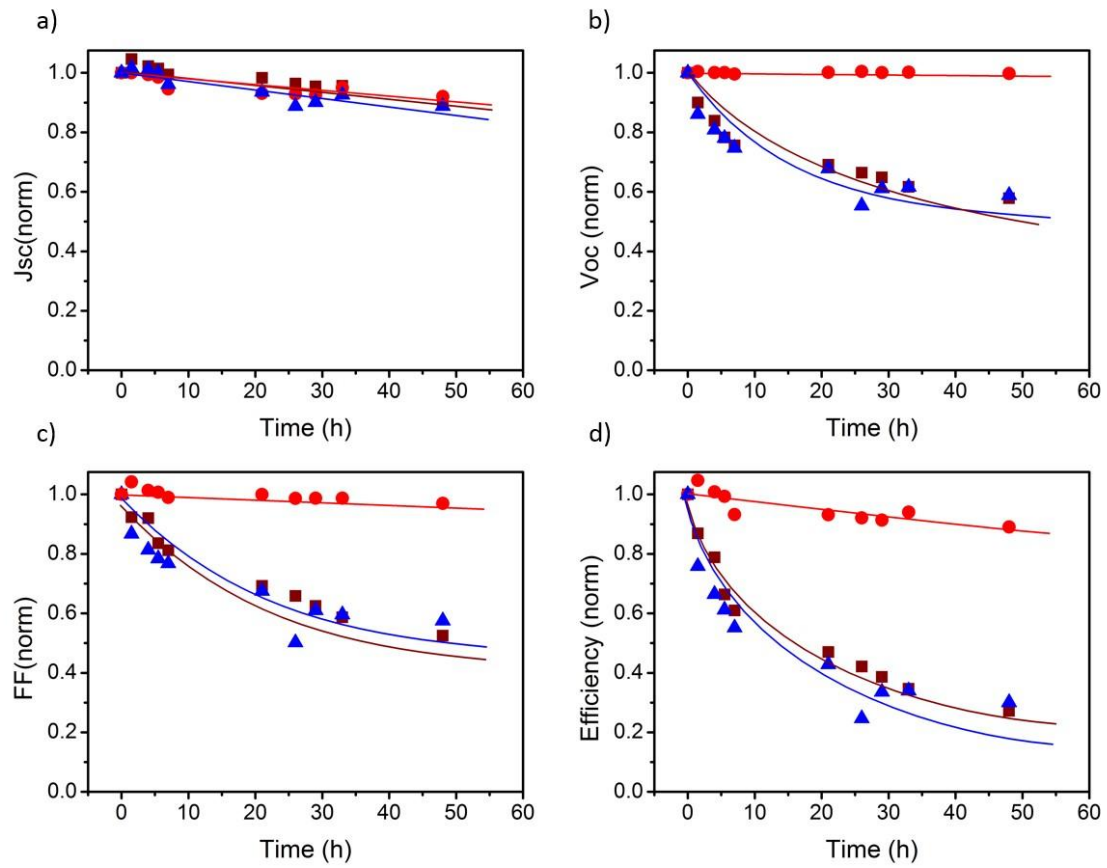


Fig. 3 Evolution of the PV parameters for Std-Opaque (Wine squares), Std-ST (Blue triangles), and Inv-ST (red circles) solar cells. All parameters are normalized to their respective value at t=0 h. The lines are guides for the eye.

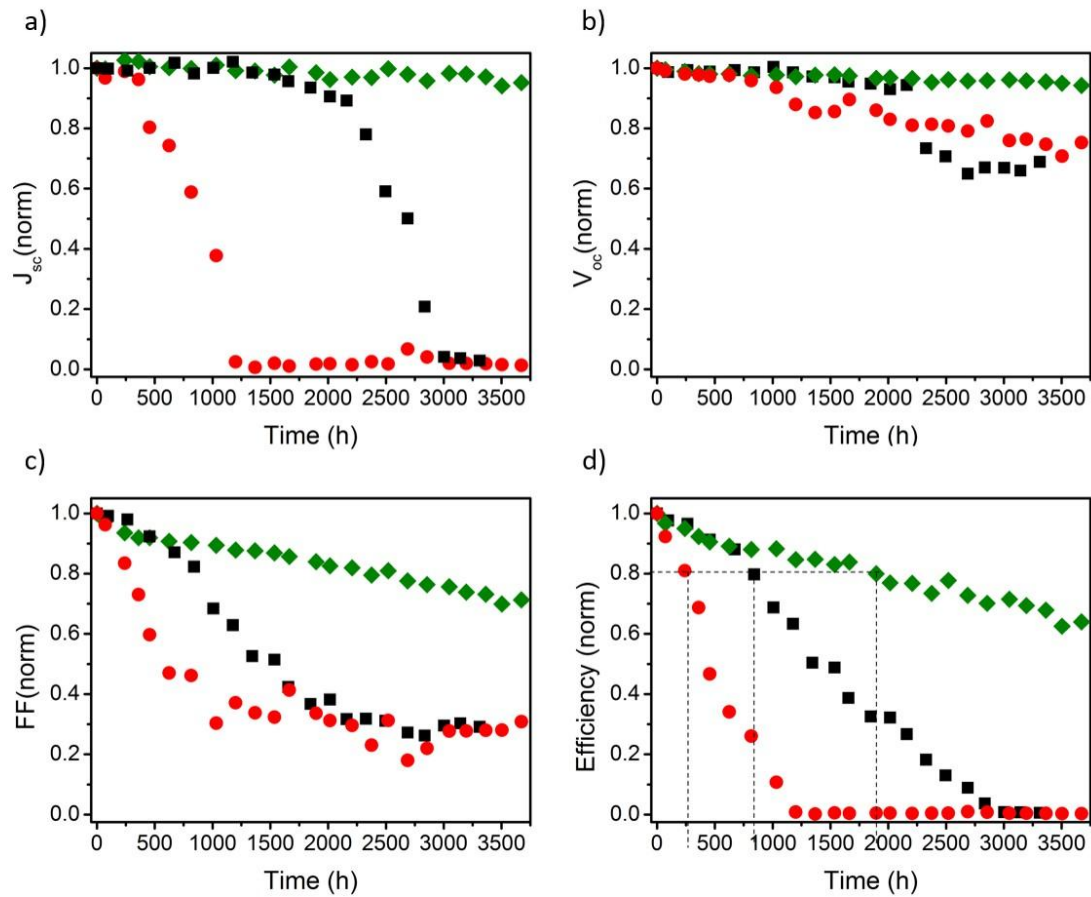


Fig. 4 Evolution of the normalized PV parameters for Inv-Opaque (black squares), Inv-ST (red circles) and ML-ST (blue diamonds) cells: J_{sc} (a), V_{oc} (b), FF (c), and Eff (d) All parameters are normalized to the respective value at $t = 0h$. The dotted lines in (d) indicate the time at which the efficiency is 80% of the initial value. The life-times of the Inv-ST/Inv-Opaque/MS-ST cells were approximately 250/750/1900 h.

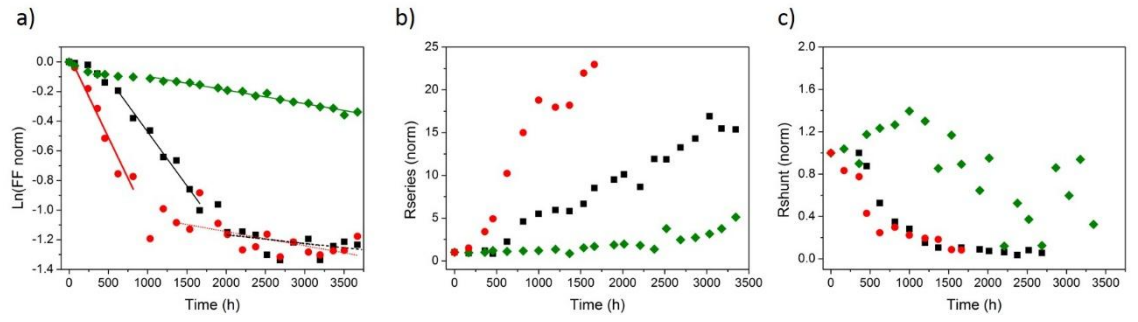
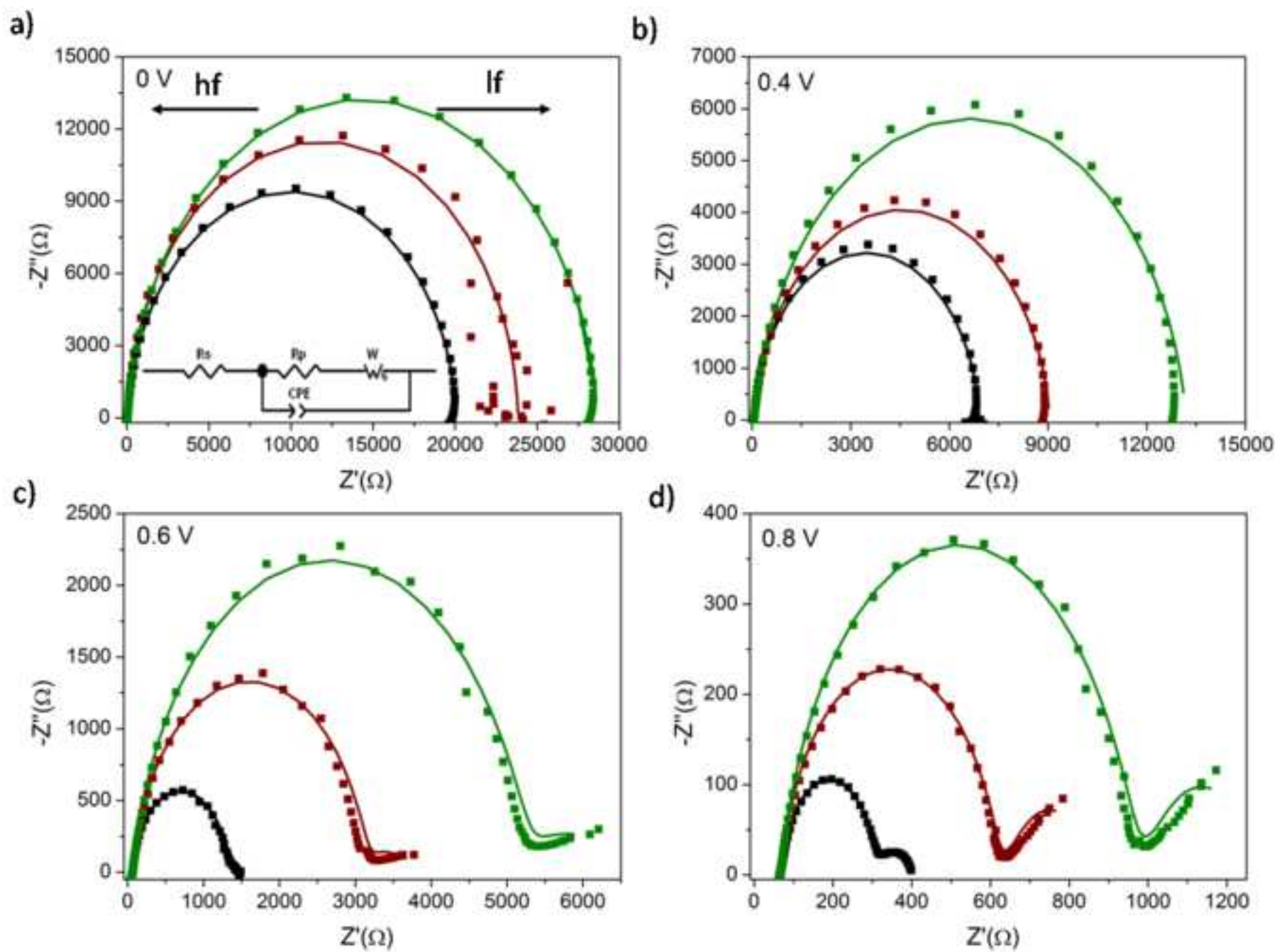


Fig. 5 Evolution of the (a) natural logarithm of the cell FF, (b) the series resistance and, (c) the shunt resistance for Inv-Opaque (black squares), Inv-ML-ST (green diamond), and Inv-ST (red circles) solar cells.

Figure
[Click here to download high resolution image](#)



Supplementary Interactive Plot Data (CSV)

[Click here to download Supplementary Interactive Plot Data \(CSV\): Supplementary data.docx](#)